metals

MDPI

Article

The High-Temperature Creep Behavior of In-Situ TiB_2 Particulate Reinforced Al12Si4Cu2NiMg Composite

Shihan Dai [1,2], Zeyu Bian [1], Mingliang Wang [1,*], Yi Wu [2], Dong Chen [2,3,*], Hongping Li [4] and Haowei Wang [2]

1 School of Materials Science and Engineering, Shanghai Jiao Tong University, No. 800 Dongchuan Road, Shanghai 200240, China; heydoris7@sjtu.edu.cn (S.D.); zybian@sjtu.edu.cn (Z.B.)
2 State Key Laboratory of Metal Matrix Composites, Shanghai Jiao Tong University, No. 800 Dongchuan Road, Shanghai 200240, China; eagle51@sjtu.edu.cn (Y.W.); hwwang@sjtu.edu.cn (H.W.)
3 Anhui Province Engineering Research Center of Aluminium Matrix Composites, Huaibei 235000, China
4 Shanghai Aircraft Design and Research Institute, Shanghai 201203, China; lihongping@comac.cc
* Correspondence: mingliang_wang@sjtu.edu.cn (M.W.); chend@sjtu.edu.cn (D.C.); Tel.: +86-21-3420-2540-203 (M.W.); +86-21-5474-7597-202 (D.C.)

Received: 9 October 2018; Accepted: 3 November 2018; Published: 7 November 2018

Abstract: In the present work, the in-situ TiB_2/Al12Si4Cu2NiMg (denoted as 'Al-12Si') composites were successful synthesized through the salt-metal reaction route. The influences of weight fraction (0, 4, and 9 wt.%) and heat treatment (T5 and T7) on the tensile creep deformation were studied at $\geq$623 K under constant load in air. At the investigated temperature and stress condition, TiB_2 particles increased creep deformation resistance, as compared to the unreinforced alloy, while the composites presented similar strength when the weight fraction of reinforcement increased from 4% to 9%. It was found that the steady-state creep rate was lower in the 4 wt.% TiB_2/Al-12Si composite (T5), as compared with that in the 4 wt.% TiB_2/Al-12Si composite (T7). The result has been rationalized by using the load-partitioning model and relative to the evolution of the rigid phase. The creep deformation of the 4 wt.% TiB_2/Al-12Si composite was controlled by the climb of dislocations in the aluminum alloy matrix.

Keywords: Al matrix composites; nano particles; creep; load transfer

1. Introduction

Discontinuously reinforced aluminum matrix composites (DRAMCs) have received growing interests as the potential structural materials for high-temperature applications, such as aerospace, automotive, and manufacturing fields, due to their high specific strength, modulus, and several other favorable characteristics [1–7]. However, the creep deformation at high temperatures, generally above 473 K, for DRAMCs, may lead to failures [8]. Hence, further investigations on long-term exposure are required to ensure the reliability and security of DRAMCs in service [9].

Extensive investigations have provided information for the creep characteristics of the DRAMCs, including the profile of the creep curve [4,10–13], the stress dependence of creep rate [5,10–16], the temperature dependence of creep rate [5,10–12,15], and the evolution of creep microstructure [4,5,17,18]. Nevertheless, the creep response may differ from one composite to another, and should be correlated to the fabrication process and test conditions. For example, the influence of reinforcement is variable. The composites, reinforced by nano-sized TiC*x* particles, has been reported by Wang et al. [19], with about 4–15 times higher creep resistance ability than those of the unreinforced matrix alloy. On the other hand, the presence of the reinforcement, in some cases, may be detrimental by preferentially promoting damage [20,21], such as acting as dislocation

sources [22,23]. Requena et al. [14] has showed the considerably lower creep resistance of 22 vol.% Al_2O_3/AA6061 composites compared with that of the unreinforced matrix. The role played by particulate reinforcement, especially in nano-scale size, during creep is still not well understood.

Furthermore, little attention has been paid to the influence that heat treatment may have on the creep strength of the composite, although the work on the Al12SiCuMgNi alloy [24] has suggested that heat treatment affected the creep resistance of the material directly. Besides, the major creep researches are conducted on the DRAMCs, which are typically fabricated by powder metallurgy (PM). The PM processed DRAMCs have always shown higher creep resistance and more regular experimental data compared to the ingot metallurgy (IM) method [13,25]. However, the IM process is widely used and continuously developed due to its ability to achieve high part volumes and tight part tolerances at lower cost in the industrial application [26]. The study of creep behavior for the IM DRAMCs has been largely neglected by the academia.

The present study is aiming to understand the steady state creep behavior and fracture mechanism of in-situ TiB_2/Al12Si4Cu2NiMg composite produced by the IM strategy. The study consists of two sections. In Section 1, the similarities and differences in the creep behaviors between composites and the alloy as well as the relevant creep mechanisms, such as the role of the particle reinforcement, are identified and discussed. In Section 2, the analysis, based on the concept of load transfer, has been proposed to describe the creep behavior of the composite at different heat-treated states.

2. Materials and Methods

2.1. Materials

In this work, an Al12Si4Cu2NiMg alloy (hereafter denoted as 'Al-12Si alloy') and two Al-12Si alloy matrix composites reinforced with 4 wt.% and 9 wt.% of particulate TiB_2 were used. The nominal chemical composition of the Al-12Si alloy is given in Table 1.

Table 1. Chemical composition of Al-12Si matrix alloy (wt.%).

Si	Cu	Ni	Mg	Fe	Mn	Ti	Al
12.3	3.86	1.98	0.93	0.5	0.115	0.009	Bal.

The $x$$TiB_2$/Al-12Si composites ($x$ = 4 and 9 wt.%) were produced by adding the pre-weighted mixture salts of K_2TiF_6 and KBF_4 into the Al-12Si alloy melt at 1123 K through the exothermic reaction. The ratio of K_2TiF_6 and KBF_4 was 1:2. The melt was stirred using a blade paddle mixer, and then slag was skimmed out completely [1,27–29]. Finally, the melt was poured into the pre-heated molds to achieve the as-cast ingots.

2.2. Heat Treatment

For the T5 heat treatment, both the as-cast composites and the Al-12Si alloy were artificially aged at 473 K for 4 h to achieve the T5 condition. Regarding the T7 heat treatment, the 4 wt.% TiB_2/Al-12Si composite was subjected to solution treatment at 783 K for 3.5 h, and quenched into water. Lastly, the samples were artificially aged at 503 K for 7 h, and cooled in the air successively.

2.3. Creep Testing

The preparation of samples and the process of creep experiments were according to the uniaxial creep testing method in tension for metallic materials (GB/T 2039-2012). The sheet tensile creep specimens with 2 mm in thickness and 25 mm in gauge length were used. Tests were carried out at 623 K under the constant load in the range of 30 to 45 MPa on the creep machine (RDL50, ZhongJi Corp., Changchun, China). Before loading the samples into the facility, all samples were carefully polished in order to minimize the influence of machining defects. The temperature of the specimens was

monitored by three separate thermocouples placed at the middle and two ends of the gauge length accordingly. The temperature was held within ±2 K during the tests. Strains were measured using two extensometers, and the data acquisition was carried out every 60 s during the whole test. All samples were stabilized at the target temperature for 1 h prior to testing.

2.4. Microstructure Characterization

The microstructure characterization was carried out by optical microscopy (OM, Axio Imager, Zeiss Corp., Oberkochen, Germany) and scanning electron microscopy (SEM, MAIA3, Tescan Corp., Brno, Czech Republic) equipped with the energy dispersive spectroscopy (EDS, Bruker Corp., Rheinstetten, Germany). The phase constitutions of the materials were identified using a poly-functional X-ray diffractometer (XRD, D8 ADVANCE Da Vinci, Bruker Corp., Rheinstetten, Germany) with Cu Kα radiation setting in the 2θ range of 10° to 90° at a scanning speed of 2° min^{-1}.

3. Results

3.1. Microstructure

Figure 1 shows the XRD spectra of the in-situ xTiB$_2$/Al-12Si composites (x = 0, 4 and 9 wt.%) at T5 states and the in-situ xTiB$_2$/Al-12Si composites (x = 4 wt.%) at T7 state. The spectra of composites can all be indexed to Al, Si, and TiB$_2$. The presences of intermetallic compounds (e.g., Al_3CuNi, $Al_5Cu_2Mg_8Si_6$, and Mg_2Si) are also evident in the XRD patterns.

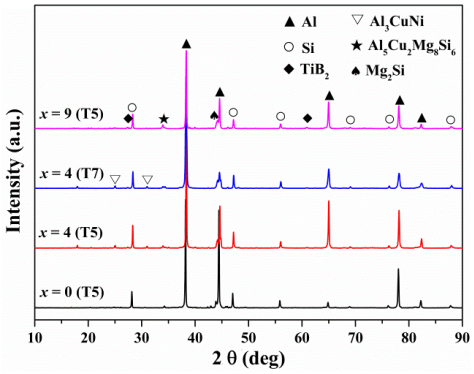

Figure 1. XRD spectra of the in-situ xTiB$_2$/Al-12Si composites (x = 0, 4 and 9 wt.%, T5) and the in-situ xTiB$_2$/Al-12Si composites (x = 4 wt.%) at T7 state.

Figure 2a–d show the optical micrographs of the Al-12Si alloy (T5), the 4 wt.% TiB$_2$/Al-12Si composite in both T5 and T7 states, and 9 wt.% TiB$_2$/Al-12Si composite (T5) accordingly. Qualitatively, the size of primary Si at T5 state (Figure 2b) is similar to that at T7 state (Figure 2c) for the 4 wt.% TiB$_2$/Al-12Si composite. Notably, the morphology of eutectic Si changes in these materials at different states. The lamellar eutectic Si, which is actually a network structure in three dimensions, form and are observed in T5 condition (Figure 2b), but disintegrate and become rounder in T7 state (Figure 2c). An aggregation of the primary Si phase with the largest size are in the order of ~100 μm, and a clear spheroidization of the eutectic Si is observed in the 9 wt.% TiB$_2$/Al-12Si composite (Figure 2d).

The SEM micrographs of xTiB$_2$/Al-12Si composites (x = 4 and 9 wt.%) in their T5 states are exhibited in Figure 3a,b,e. Figure 3a shows the numerous intermetallic compounds consisting of Cu- and Ni-rich phases (e.g., Al_3CuNi), Mg_2Si, and Q-$Al_5Cu_2Mg_8Si_6$, which is in good consistency with the results shown in the XRD spectra (Figure 1). Theses phases are beneficial to improve the high temperature strength of Al based materials [30]. Meanwhile, the TiB$_2$ particle cluster has been reported as a common phenomenon during the casting of Al-based composites [1,31]. Figure 3b shows the distribution of TiB$_2$ particle clusters in 4 wt.% TiB$_2$/Al-12Si composite. The TiB$_2$ particle clusters are mainly co-existing with the Si phase at grain boundaries, and the distribution of the TiB$_2$ particulates

is relatively uniform throughout the matrix (Figure 3b). Figure 3c shows the typical morphology of TiB_2 particles with near-spherical, hexagonal, or quadrilateral shapes [27]. Figure 3d illustrates the size distribution of TiB_2 particles in the 4 wt.% TiB_2/Al-12Si composite. The size of the TiB_2 particles ranges from 30 nm to more than 500 nm. The number of the particles decreases by increasing particle size to 500 nm. Notably, nearly half of the particles are 30–100 nm in size. Figure 3e shows the distribution of TiB_2 particle clusters in the 9 wt.% TiB_2/Al-12Si composite. The TiB_2 particle aggregates significantly as the amount of TiB_2 particles increases to 9 wt.%. The TiB_2 particle clusters have spread over the matrix with the size up to ~40 μm (Figure 3e).

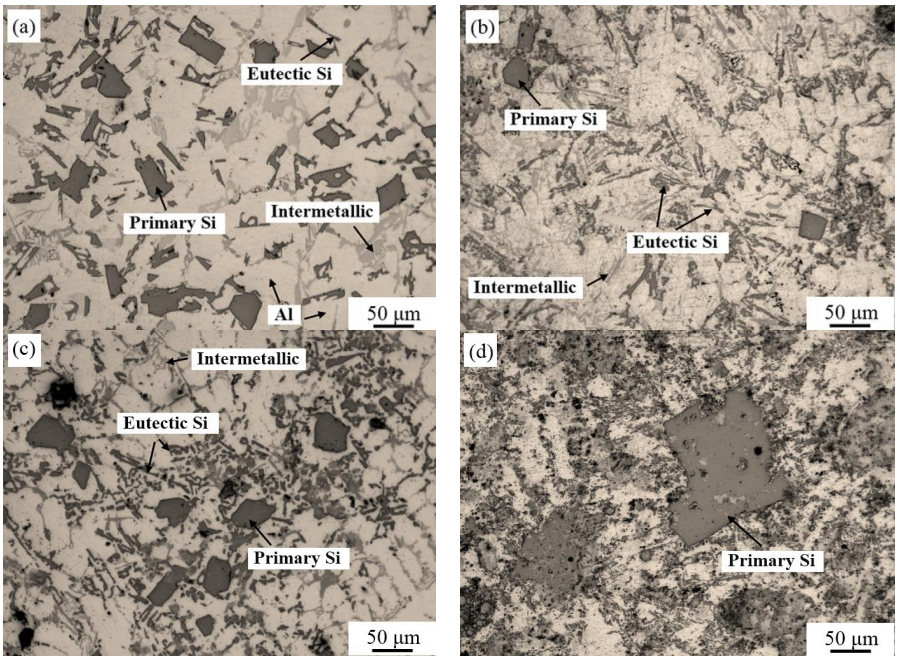

Figure 2. Optical micrographs of (**a**) Al-12Si alloy (T5); (**b**) 4 wt.% TiB_2/Al-12Si composites (T5); (**c**) 4 wt.% TiB_2/Al-12Si composites (T7); and (**d**) 9 wt.% TiB_2/Al-12Si composites (T5).

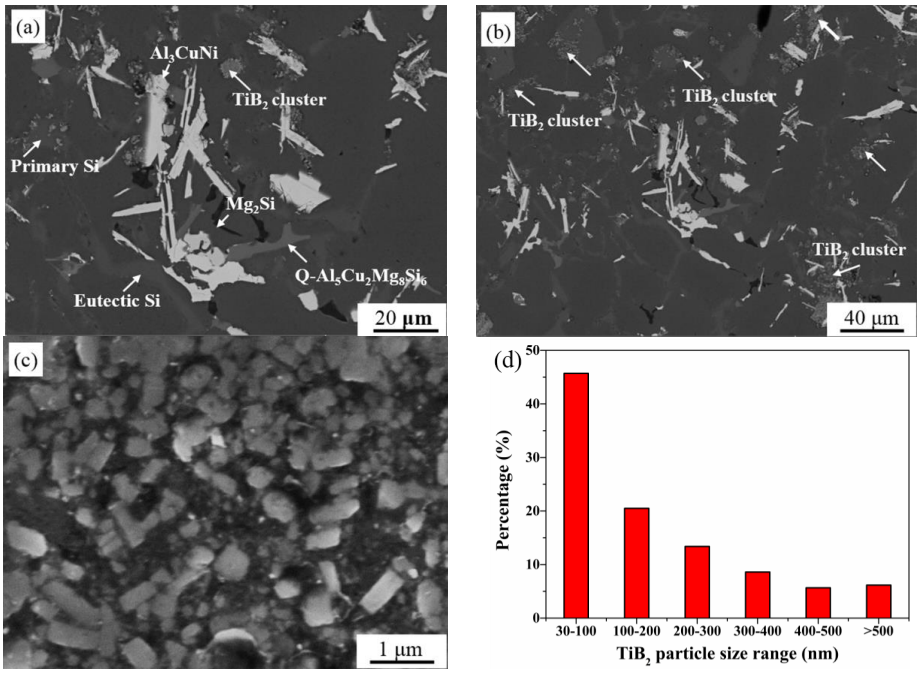

Figure 3. *Cont.*

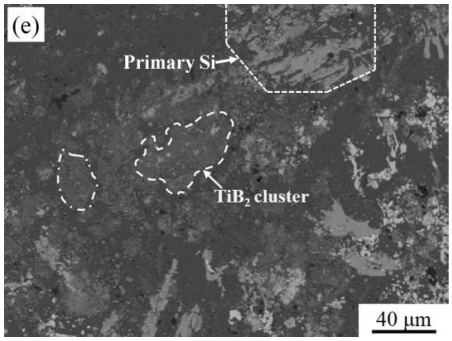

Figure 3. SEM micrographs of 4 wt.% TiB_2/Al-12Si composite (**a**) intermetallics; (**b**) the distribution of TiB_2 particle clusters; (**c**) typical morphology of TiB_2 particles; (**d**) TiB_2 particle size distribution and 9 wt.% TiB_2/Al-12Si composite; (**e**) the distribution of TiB_2 particle clusters at T5 state.

3.2. Creep Curves

The study of the creep behavior for materials in the laboratory condition is often based on the uniaxial tensile creep test. A typical creep curve in the form of strain (ε) versus time (t) can be achieved first. Then, the slope of the curve at a specific position denotes the instantaneous creep rate ($\dot{\varepsilon}$) at the corresponding moment.

Figure 4a shows the creep curve for the composite using the 4 wt.% TiB_2/Al-12Si composite (T5) as an example. In order to compare the creep stages for materials, under different creep life, the creep life fraction is used to substitute the creep time. The three stages can be evidently observed from the creep curve of instantaneous strain rate versus the creep life fraction (Figure 4b).

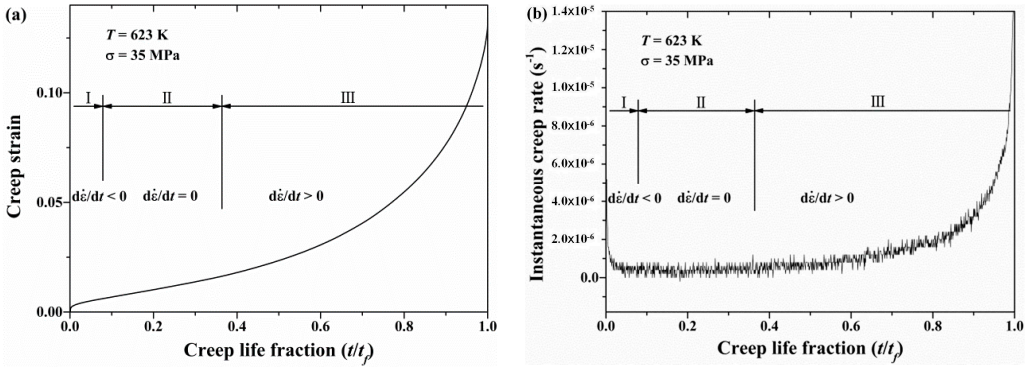

Figure 4. Creep curve of (**a**) creep strain versus creep life fraction and (**b**) instantaneous creep rate versus creep life fraction for 4 wt.% TiB_2/Al-12Si composite (T5) at 623 K under an applied stress of 35 MPa.

Normally, the creep curve exhibits three stages [32]:

(a) Stage I (a short primary stage): The deformation resistance is low, and the instantaneous creep rate decreases continuously with time ($d\dot{\varepsilon}/dt < 0$) due to the work hardening behavior.

(b) Stage II (a moderate secondary stage): The instantaneous creep rate reaches its minimum value and remains constant ($d\dot{\varepsilon}/dt = 0$), denoting the dynamic equilibrium during deformation process. The Stage II is the focus of the researches. The constant creep rate in Stage II, usually called the steady-state creep rate ($\dot{\varepsilon}_{ss}$), is an important parameter to compare the creep resistance of the materials [23]. However, for some materials, the Stage II is short, and the steady-state creep rate can not be well defined. Then, the minimum creep rate ($\dot{\varepsilon}_{min}$) is preferably used for the study [13,33,34]. Generally speaking, there is little distinction between the steady-state creep rate ($\dot{\varepsilon}_{ss}$) and the minimum creep rate ($\dot{\varepsilon}_{min}$) [19,35,36]. In the present work, the creep rate refers to the steady-state creep rate unless otherwise specially illustrated.

(c) Stage III (an extended tertiary stage): The instantaneous creep rate increases ($d\dot{\varepsilon}/dt > 0$) until rupture, and is usually related to the advent of damage in the material.

Figure 5 presents the typical creep curves of these four materials in the form of strain (ε) verus time (t) under an applied stress of 35 MPa. Several creep data can be achieved for contrast, including the creep life, the creep rate, and the strain-to-failure. All composite materials exhibit higher creep resistance (i.e., lower creep rates and longer lifetime) than the alloy counterpart. However, the 4 wt.% TiB_2/Al-12Si composite (T5) and 9 wt.% TiB_2/Al-12Si composite (T5) have exhibited similar creep rates. Namely, the variation in the weight fraction of TiB_2 particles shows a negligible effect on creep strength. Besides, it is noted that 9 wt.% TiB_2/Al-12Si composite (T5) shows a lower lifetime than 4 wt.% TiB_2/Al-12Si composite (T5) at 35 MPa. Finally, a higher creep rate is observed in the 4 wt.% TiB_2/Al-12Si composite (T7) compared to that in the 4 wt.% TiB_2/Al-12Si composite (T5). Similar variation tendencies in the creep rates are available over the entire stress range used.

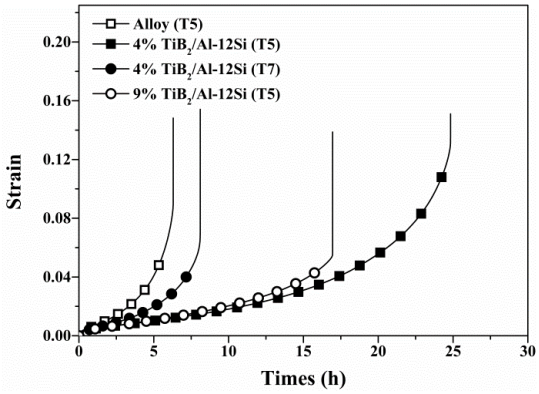

Figure 5. Typical creep curves for all materials at 623 K under an applied stress of 35 MPa.

Table 2 summarizes the proportion of three stages for xTiB$_2$/Al-12Si composites (x = 4 and 9 wt.%) and the Al-12Si alloy at 623 K. The careful inspection of the creep values in this table has lead to two conclusions.

Table 2. The proportion of three phases for xTiB$_2$/Al-12Si composites (x = 4 and 9 wt.%) and the Al-12Si alloy at 623 K.

Samples	Applied Stress (MPa)	Stage I (%)	Stage II (%)	Stage III (%)
Al-12Si alloy (T5)	30	8	20	72
	35	8	16	76
4 wt.% TiB_2/Al-12Si composite (T5)	30	5	40	55
	35	7	29	64
	40	9	23	68
	45	12	16	72
4 wt.% TiB_2/Al-12Si composite (T7)	30	8	30	62
	35	9	27	64
	40	10	16	74
	45	13	14	73
9 wt.% TiB_2/Al-12Si composite (T5)	30	4	57	39
	35	7	31	62
	40	9	22	69
	45	11	15	74

(1) For all materials, Stage I shows the relative stable or slight increased proportions over the whole stress range. In Stage II, a significant reduction in this proportion has been observed with the increasing stress. In Stage III, a clear rise in the proportion is identified with the increasing stress.

Finally, the results have indicated that the shapes of the creep curves for studied Al-12Si based materials are dependent of the test load.

(2) The Stage II is well-defined for both the composites and the Al-12Si alloy. For Al-12Si alloy, the Stage II occupies 15–20% of the whole creep life. For 4 wt.% TiB_2/Al-12Si composite (T5), the Stage II occupies 15–40% of the whole creep life. Finally, the $x$$TiB_2$/Al-12Si composites ($x$ = 4 and 9 wt.%) show a higher proportion of the Stage II compared with that of the Al-12Si alloy.

The performance during creep process is relative with the creep mechanism. For Al-based composites, the dislocation creep or the constant structure model is most reported [2,5,10,11,18,19,37]. From a viewpoint of dislocation creep, dislocation multiplication occurs in Stage I with materials hardening. Then, the recovery softening occurs by dislocation climb. The Stage II is an equilibrium process of the dislocation glide and dislocation climb. The present result reveals that, in the lower stress range, Stage II for composites is evident. This feature may be related to the TiB_2 particles. The reinforcements can work as dislocation obstacles to maintain the creep deformation. Therefore, the duration of Stage II prolongs accordingly. It can also explain why the composites have a higher proportion of Stage II over the alloy. However, Stage II has a shorter time in the higher stress range.

The features for the creep curves in composites are similar to those for 10 wt.% TiB_2/ZL109 composite [2], 15 vol.% TiB_2/Al composite [19], 15 vol.% SiC/8009 Al [20], and the Al-Cu composites reinforced with 11.1 vol.% Al_2O_3 and 8.9 vol.% TiB_2 [21], which have reported a clear Stage II with about 25–40% of the whole creep life. In contrast, the various creep data for DRAMCs [12,38,39] also revealed a short and poorly defined duration of secondary stage. Besides, the feature for the studied Al-12Si alloy is also, to some extent, different from what was reported for the unreinforced Al alloy, i.e., ZL109 [2], 2124 Al [11], and 2024Al [34], which has been stated as a parabola shape creep curve under the test conditions. The present results have indicated that the brief Stage II is not an intrinsic property of all DRAMCs and corresponding alloys, as reported in Reference [32]. Unfortunately, the relative rules in the characteristics of creep curves is still unclear.

Finally, it is noted that the three stages for both the 4 wt.% TiB_2/Al-12Si composite (T5) and the 9 wt.% TiB_2/Al-12Si composite (T5) should account for the similar proportion, except in the case under 30 MPa. The result further reveals the similarities in creep curves for the two composites and correspond with the previous observation (Figure 5). However, the difference under the lowest stress is unusual.

Figure 6 represents the comparison of the creep curves for the Al-12Si composite reinforced with 4 wt.% and 9 wt.% TiB_2 (T5) under an applied stress of 30 MPa. The Stage II occupies over half of the whole life for 9 wt.% TiB_2/Al-12Si composite, which is significantly higher than that for 4 wt.% TiB_2/Al-12Si composite.

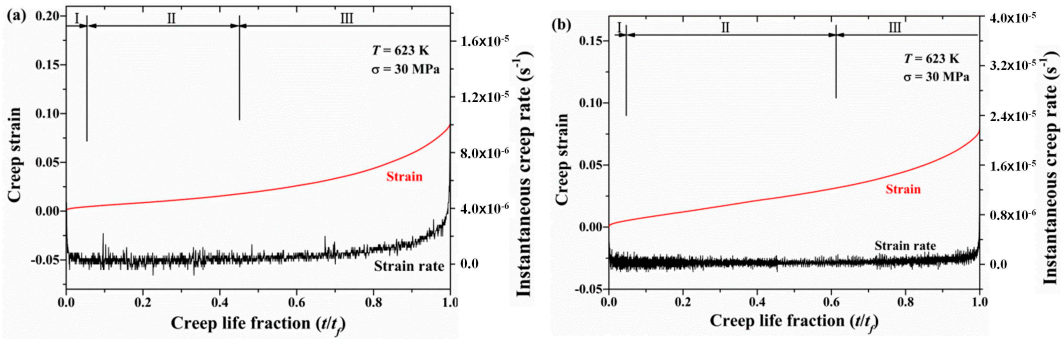

Figure 6. Creep curves for (**a**) 4 wt.% TiB_2/Al-12Si and (**b**) 9 wt.% TiB_2/Al-12Si composites (T5) at 623 K under an applied stress of 30 MPa.

Table 3 lists the specific creep test results for the $x$$TiB_2$/Al-12Si composites ($x$ = 4 and 9 wt.%) under 30 MPa. The creep life for two composites is 35.1 h and 51.7 h, respectively. According to the data in Table 2, the actual durations of Stage I and Stage III are 21.06 h and 22.23 h. In other

words, both materials undergo similar creep courses, and the longer creep life for 9 wt.% TiB_2/Al-12Si composite is attributed to the longer Stage II. Stage II has been reported as an important stage during creep, as mentioned above, and should be relevant to the creep life. Therefore, two speculations may be accounted for in the present result. One is relative to the high weight fraction of TiB_2 reinforcements. On the other hand, it is noted that the applied stress is low, which may indicate that a superior creep resistance can be achieved for 9 wt.% TiB_2/Al-12Si composite as the stress decreases.

Table 3. The creep test results for the $x$$TiB_2$/Al-12Si composites ($x$ = 4 and 9 wt.%) at 623 K under an applied stress of 30 MPa.

Samples	Creep Life (h)	Proportion of the Stage I and Stage III (%)	Duration of the Stage I and Stage III (h)
4 wt.% TiB_2/Al-12Si composite (T5)	35.1	60	21.06 [1]
9 wt.% TiB_2/Al-12Si composite (T5)	51.7	43	22.23 [2]

[1] 0.6 × 35.1 h = 21.06 h; [2] and 0.43 × 51.7 h = 22.23 h.

4. Discussion

4.1. The Influences of TiB_2 Particles and Si on the Creep Behavior

Based on the experiment results, the difference in creep behavior of 4 wt.% TiB_2/Al-12Si composites and Al-12 alloy is discussed. The matrix alloys and the heat treatment for both materials are equal, and similarly, the intermetallics should not be the main factor to make the difference. The creep improvement exhibited by the composites has obviously signified the effect of ceramic particulate on creep behavior. These improvements have been discussed by several researchers [37,40], and are attributed to both direct and indirect strengthening effects, which are introduced by the reinforcement [23,40].

Firstly, it is the deformation within the matrix that controls the creep of composite [37,41,42]. On the one hand, the reinforcement affects the microstructures of the matrix. For example, the reinforcement can work as a refiner or a pinner to keep a stable substructure, belonging to the indirect strengthening [23]. On the other hand, the direct strengthening occurs when the load transfers from the matrix to the reinforcement. Such transfer has been caused by both elastic and plastic misfit between two phases, thereby leading to a lower stress in matrix than applied stress (σ) [9,22,40].

The load transfer process can be briefly described by following the expression promoted by Fernández and González-Doncel [25]:

$$\overline{\sigma}_M(1-f)+\overline{\sigma}_R f_{eff}=\sigma, \quad (1)$$

$$\overline{\sigma}_M=\sigma-(\overline{\sigma}_R-\overline{\sigma}_M)f_{eff}=\sigma-\sigma_T, \quad (2)$$

where $\overline{\sigma}_M$ and $\overline{\sigma}_R$ are the average stress on the matrix and reinforcement, relatively; σ_T is the extra stress born by the reinforcement; and f_{eff} is the effective volume fraction of reinforcement [43].

The Equations (1) and (2) denote the average stress on the matrix ($\overline{\sigma}_M$), which is lower than the applied stress (σ) due to the extra stress borne by the reinforcement. The extra stress is relative with the effective volume fraction of reinforcement, especially for the fiber reinforcement. Moreover, for particle-reinforced composites, a high load-transfer efficiency is usually expected in the case of the a fine size of particles, high volume fraction of particles [9], a distinct difference of Young's modulus between matrix and reinforcements [22], or a strong and clean bonding [44] at the interface, which has been achieved. Ji et al. [5] have studied the compressive creep behavior of xTiC/2618Al (x = 15 and 20 vol.%) and the corresponding unreinforced alloy at the temperatures of 523, 573, and 623 K. The value of Young's modulus for TiC is 451 GPa [44]. The TiC particles were in-situ fabricated with about 0.5–1.5 μm in size, and homogeneously distributed in the Al matrix. It was shown that the creep

strength of the composites was always superior to that of the unreinforced alloy, and the composite with 20 vol.% TiC was slightly more creep resistant than that with 15 vol.% TiC [45].

In this work, the TiB_2 particles are nano-sized and bond closely with the matrix (Figure 3b,d). The Young's modulus for TiB_2 is 551 GPa [44], and the Young's modulus for Al is about 72 GPa. Therefore, it has permitted the obvious effect of TiB_2 particle on the creep behavior. In this situation, it is expected that a higher creep strength should also be achieved for the composite with higher TiB_2 weight fraction, as reported by Ji et al. [5]. However, the present result reveals similar creep rates for both 4 wt.% TiB_2/Al-12Si and 9 wt.% TiB_2/Al-12Si composites (T5). One possible reason is related to the severe TiB_2 particle clusters shown in 9 wt.% TiB_2/Al-12Si composite (T5, Figure 3c). On the one hand, the effective volume fraction of nano-sized reinforcements should be reduced, since the TiB_2 particulates agglomerate form clusters [46]. On the other hand, the severe TiB_2 particle clusters can cause the growth of voids to encourage crack initiation and propagation [46,47].

Figure 7 compares the fracture surfaces of 4 wt.% TiB_2/Al-12Si composite (T5) and 9 wt.% TiB_2/Al-12Si composite (T5). Both fracture surfaces are composed mostly of dimples with the TiB_2 particle clusters inside. The dimples result from the formation, growth, and coalescence of voids [14]. Clearly, the dimples are more homogeneous in 4 wt.% TiB_2/Al-12Si composite (T5, Figure 7a). On the contrary, the dimples are irregularly distributed in 9 wt.% TiB_2/Al-12Si composite (T5). The presence of severe clusters (marked by arrow) has caused the irregular dimples with varying sizes, indicating the detrimental influence to the creep resistance.

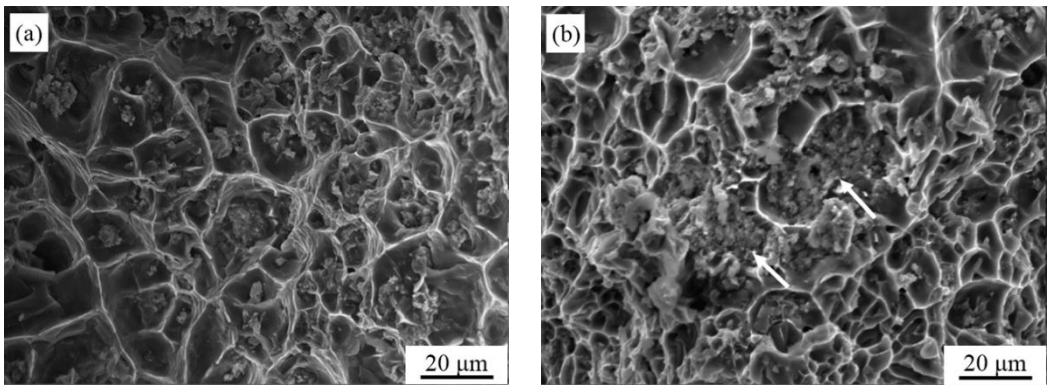

Figure 7. SEM images of fracture surfaces of (**a**) 4 wt.% TiB2/Al-12Si composite (T5) and (**b**) 9 wt.% TiB2/Al-12Si composite (T5) tested at 623 K with the TiB2 particle clusters in the dimples.

In addition, the size of the primary Si particles can be related to the creep performance, especially in Stage III [26,48]. The Si particle is a brittle phase and is susceptible to fracture during creep deformation. Meanwhile, the generation of damage processes, i.e., particle cracking or cavitation, usually turns the creep deformation into Stage III [6,49]. Figure 8 shows the fracture surfaces of two composites tested at 40 MPa. The black zones, marked by a circle (Figure 8c), are actually coarse primary Si aggregations, as shown in Figure 8d. It is obvious that the larger size of such brittle phase is detrimental to creep life. At last, the increased dislocation density at corners and edges of reinforcements may accelerate the breakdown of the brittle phase, which should reduce the creep resistance of the TiB_2/Al-12Si composite in this work [17,23]. It is noted that some of the intermetallics, such as $Al_5Cu_2Mg_8Si_6$ and Al_3CuNi, can also be observed to show the broken morphologies. The coarse intermetallic compounds may influence the creep process to some extent [48]. However, it is not the critical factor to cause creep fracture in the present study. Hence, the morphology of the intermetallic is not discussed further.

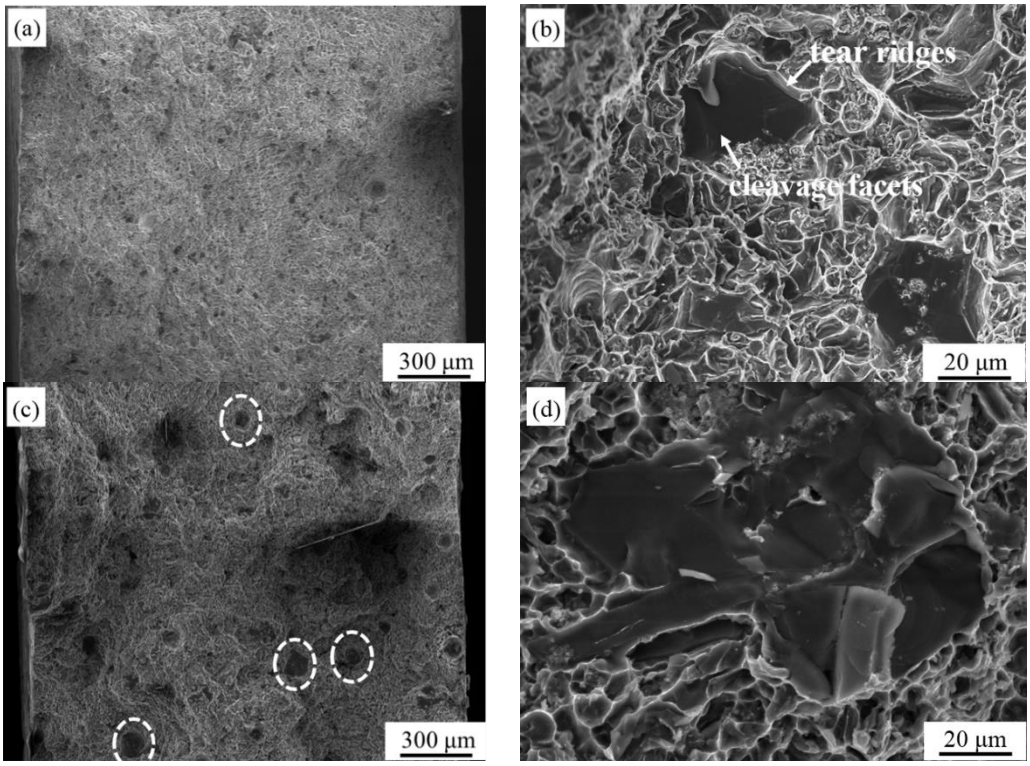

Figure 8. Overview and detailed SEM images of the tensile creep fracture surface of 4 wt.% TiB_2/Al-12Si composite (T5) (**a**) in low magnification; (**b**) in high magnification and 9 wt.% TiB_2/Al-12Si composite (T5) (**c**) in low magnification; and (**d**) in high magnification.

4.2. The Influence of Heat Treatment on the Creep Behavior

In Figure 9, the steady-state creep rate ($\dot{\varepsilon}_{ss}$) is represented as a function of σ, in a double-logarithmic scale, for the 4 wt.% TiB_2/Al-12Si composite at different heat treatments. In general, the 4 wt.% TiB_2/Al-12Si composite at the T5 state exhibited a lower creep rate compared to the T7 state. Both composites exhibit the constant power-law behavior with a similar stress exponent between six and eight in the stress range tested. This similarity may due to the dominant effect of the matrix deformation on creep behavior in the composite.

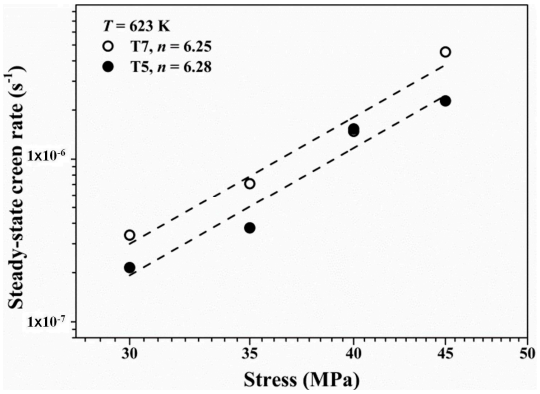

Figure 9. Steady-state creep rate as a function of the applied stress (logarithmic scale) for 4 wt.% TiB_2/Al-12Si composite at the T5 and T7 state at 623 K.

Furthermore, the concept of an effective stress [12] has been used in order to rationalize the creep behavior between two composites. For the DRAMCs, the effective stress was originally used by introducing the threshold stress (σ_0), which suggests that the observed deformation is driven by an

effective stress σ_e ($\sigma_e = \sigma - \sigma_0$) rather than the applied stress. This method has successfully modified the anomalously high value of apparent stress exponent and activation energy into reasonable levels by many authors [2,16,32,40,50]. While the characteristics of the threshold stress for the DRAMCs may still be under debate, several researchers have reached a consensus that the threshold stress originates from the interactions between dislocations and nano-scale particles (dispersoids or precipitates) [7].

The interactions are mainly connected with three deformation mechanisms: (a) The Orowan stress; (b) the back stress; and (c) the detachment stress. [32,51,52]. For the composites fabricated by PM procedures, either alloy or composite, the fine oxide particles introduced during atomization can act as effective barriers to dislocate motion. Besides this, the precipitates (i.e., θ(Al_2Cu) or S(Al_2CuMg) phases) presented in the matrix alloy [33] can also be accounted for the threshold stress. Recently, the transmission electron microscopy (TEM) observation by Erfanian-Naziftoosi et al. [48] lend support for this suggestion. However, this approach sometimes fails to explain the meaning of σ_0 in the composites because many authors argued that the reinforcing particles are too large to apply relevant models [25].

As mentioned above, as a clearer and simpler concept, load transfer is proposed subsequently and is used to explain the creep of the Al composites either together with σ_0 or alone [18,33,41]. In this work, it is noted that the 4 wt.% TiB_2/Al-12Si composites have been fabricated in-situ with size in the nanometer range. In addition to the precipitates in the matrix alloy, these fine TiB_2 particles can be responsible for the origin of the threshold stress. As a result, the power law creep equation, after taking a threshold stress into consideration, has been modified in the following form:

$$\dot{\varepsilon}_{ss} = A\left(\frac{\sigma - \sigma_0}{E}\right)^n exp\left(-\frac{Q}{RT}\right), \quad (3)$$

where A is a structure sensitive material constant; E is Young's modulus; R is ideal gas constant; T is the absolute temperature; Q is the activation energy for creep; n is the stress exponent.

The threshold stress can be estimated by the direct extrapolation method used in most works [5–7,12,51,53]. The stress exponent n (= 3, 5, 8) is chosen priori, and $\dot{\varepsilon}_{ss}^{-1/n}$ is plotted against σ. Different values of n correspond to the different dominant mechanisms in creep deformation: n = 3 is for the case in which the creep is controlled by viscous glide of dislocation [5], n = 5 represents the creep is controlled by the high temperature climb, and a constant structure model generates when n = 8 [2]. The value of n is confirmed when a linear relationship is observed. Meanwhile, the value of threshold stress is equal to the intersection with the horizontal axis of zero strain rate by linear extrapolation.

From Figure 10, the linear relationships were observed for both materials when n = 5, which has implied that the governing mechanism for the creep deformation should correspond to the climb of dislocations [5,33].

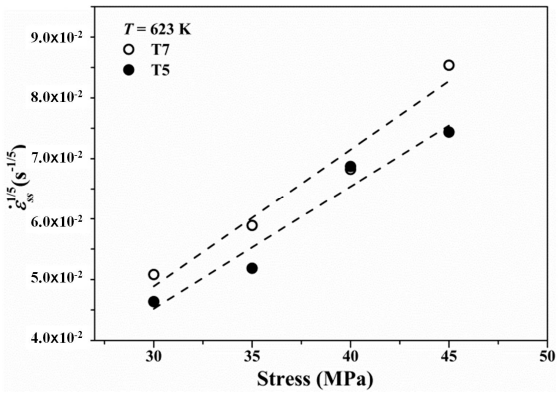

Figure 10. A plot of $\dot{\varepsilon}_{ss}^{1/5}$ vs. σ for 4 wt.% TiB_2/Al-12Si composite at both T5 and T7 states.

The threshold stress data of 4 wt.% TiB_2/Al-12Si composite (T5 and T7 states), obtained from Figure 10, are listed in Table 4. For comparison purposes, the threshold stress of the corresponding

un-reinforced alloys was also listed in Table 4. From the table, the values of σ_0 for both composites are essentially identical and higher than that for alloy. The experimental data is consistent with the inference above. Meanwhile, based on the identical volume of reinforcements, there is little difference, qualitatively, in terms of the interaction between dislocation and precipitate working at higher temperatures for both T5 and T7 heat treatments.

Table 4. Estimated values for the threshold stress (σ_0).

Temperature (K)	4 wt.% TiB_2/Al-12Si Composite (T5)	4 wt.% TiB_2/Al-12Si Composite (T7)	Al-12Si Alloy (T5)
623	9.02	9.37	4.3

As noted in the preceding section, the experimental data have indicated a similarity in creep behavior between these two composites. Meanwhile, the TiB_2 particles in both states should have little difference in direct strengthening effect. The strengthening mechanism in 4 wt.% TiB_2/Al-12Si composite at T5 state seems to be unclear.

However, researches on the Al-based composites suggested that heat treatment may influence the creep performance, mainly, in two ways: (a) The formation of fine precipitates, leading to a strong interaction between the precipitated phases and dislocations [44,48]; (b) the variation of microstructure, such as dissolution of intermetallics; or an evolution of morphology, leading to a difference in load bearing capability. Fernández-Gutiérrez and co-workers [24] investigated the high temperature creep behavior of a cast Al12SiCuMgNi piston alloy under different heat treatment. They indicated that the skeleton structure began to collapse and load transfer tended to lose as the solution heat treatment time increased. The highest creep strength was achieved in as-cast condition.

Hence, the different creep behaviors of 4 wt.% TiB_2/Al-12Si composites between T5 and T7 state may be due to the evolution of microstructure architecture based on the present experiment information. For the Al-12Si alloy, the Si phase, Mg_2Si and Cu-, and Ni-rich phases can act as the rigid phases to bear the load transferred from Al-matrix. Figure 11 presents the similar average size of primary Si for 4 wt.% TiB_2/Al-12Si composite at the T5 and T7 state. Nevertheless, a distinct spheroidization has been shown in Figure 2c (T7 state), as compared to Figure 2b (T5 state). On the one hand, the disintegration of Si network can reduce the load bearing capability in materials [1,24,31]. Besides this, TiB_2 particles can restrict the growth of eutectic Si and further change its morphology. On the other hand, the heat treatment may provoke the partial dissolution of Mg-rich and other intermetallic compounds. In this respect, we may need more details or experiments to clarify the specific weight fraction of evolution.

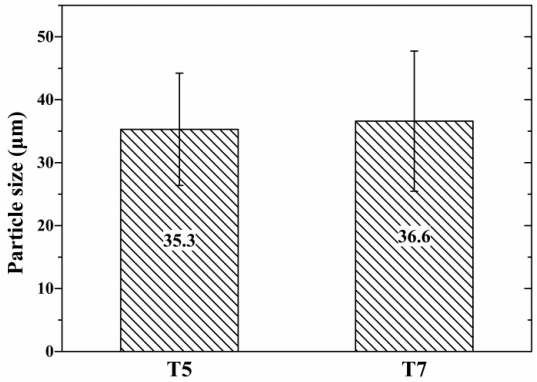

Figure 11. Average size of primary Si for 4 wt.% TiB_2/Al-12Si composite at both T5 and T7 states.

Given the above discussion, parameter α is introduced to quantitatively describe the general influence of Si phase and other intermetallics on creep strength. The parameter α is similarly used

to express the extent of load transfer in References [33,37,41]. Due to the load bearing capability of the rigid phases, the stress applied on the matrix actually equals (1–α)($\sigma - {\sigma_0}^*$). After taking the load transfer mechanism into consideration, a detailed analysis is conducted on the preceding equation. The equation has been rewritten in the form:

$$\dot{\varepsilon}_{ss} = A'\left(\frac{(1-\alpha)(\sigma-\sigma_0^*)}{E}\right)^n exp\left(-\frac{Q}{RT}\right), \quad (4)$$

where ${\sigma_0}^*$ is apparent threshold stress; α is called the load transfer coefficient.

The apparent threshold stress is numerically equal to σ_0, as listed in label 2. The origin and more details about ${\sigma_0}^*$ is not the focus in this paper and has been stated elsewhere [18,41]. Furthermore, the steady-state creep rates of the composite ($\dot{\varepsilon}_{ss,com}$) and the unreinforced matrix alloy ($\dot{\varepsilon}_{ss,alloy}$) are related, simply by using the following expression [33,41,54]:

$$\frac{\dot{\varepsilon}_{ss,com}}{\dot{\varepsilon}_{ss,alloy}} = (1-\alpha)^n, \quad (5)$$

Similarly, the expression has been modified, as follows, for 4 wt.% TiB_2/Al-12Si composite at different heat treatments:

$$\frac{\dot{\varepsilon}_{ss,T5}}{\dot{\varepsilon}_{ss,T7}} = (1-\alpha)^n \quad (6)$$

Using Equation (6), together with other experimental data obtained from Figure 10, the value of α is obtained at about 0.11. The value of α denotes the difference in the extent of load transfer between two states due to the microstructures evolution. The present analysis has explained the lower creep rate at the T5 state and should be in accordance with the microstructure observation.

5. Conclusions

The in-situ TiB_2/Al-12Si composites were successfully synthesized through the salt-metal reaction route. The work studied the constant stress tensile creep properties of the TiB_2/Al-12Si composites and the corresponding Al-12Si alloy. The main conclusions are drawn as follows:

(1) All composites show a higher creep resistance than the unreinforced matrix for the investigated test conditions. Among the composites, the Al-12Si alloy, reinforced with 4 wt.% TiB_2 particles, shows the similar creep resistance compared to that with 9 wt.% TiB_2. This may be attributed to the detrimental effects that originate from TiB_2 clusters and the coarse brittle Si phase.

(2) The threshold stress during creep deformation, measured in the TiB_2/Al-12Si composites, showed higher values than the alloy. It has indicated that the origin of the threshold stress should be related to the presence of nano TiB_2 particles.

(3) By incorporating the measured threshold stresses and load transfer into the analysis, it gives a reasonable explanation for the steady state creep behavior of the 4 wt.% TiB_2/Al-12Si composites at both the T5 and T7 heat treated states and shows a true stress exponent of n = 5. The portion of stress acting on the matrix depends on the reinforcement as well as the microstructure architecture (eutectic Si and intermetallic compounds).

Author Contributions: S.D., M.W. and D.C. performed the experiments, analyzed the data, and wrote the whole manuscript; Z.B. and Y.W. participated in the SEM experiments and image analysis; H.L. participated in the creep experiments and result analysis; H.W. participated in the revision of the manuscript; All authors had commented on the manuscript.

Funding: This research was funded by the National Key Research and Development Program of China (Grant No. 2016YFB1100103), and the project (Grant No. 2017WAMC002) sponsored by Anhui Province Engineering Research Center of Aluminum Matrix Composites (China).

Conflicts of Interest: The authors declare no conflict of interest.

References

1. Wang, M.; Chen, D.; Chen, Z.; Wu, Y.; Wang, F.; Ma, N.; Wang, H. Mechanical properties of in-situ TiB_2/A356 composites. *Mater. Sci. Eng. A* **2014**, *590*, 246–254. [CrossRef]
2. Huang, M.; Li, X.; Yi, H.; Ma, N.; Wang, H. Effect of in situ TiB_2 particle reinforcement on the creep resistance of hypoeutectic Al-12Si alloy. *J. Alloys Compd.* **2005**, *389*, 275–280. [CrossRef]
3. Kainer, K.U. *Metal Matrix Composites: Custom-Made Materials for Automotive and Aerospace Engineering*; Wiley-VCH: Weinheim, Germany, 2006; p. 300.
4. Lin, Z.; Li, Y.; Mohamed, F.A. Creep and substructure in 5 vol.% SiC-2124 Al composite. *Mater. Sci. Eng. A* **2002**, *332*, 330–342. [CrossRef]
5. Ji, F.; Ma, M.Z.; Song, A.J.; Zhang, W.G.; Zong, H.T.; Liang, S.X.; Osamu, Y.; Liu, R.P. Creep behavior of in situ TiC_P/2618 aluminum matrix composite. *Mater. Sci. Eng. A* **2009**, *506*, 58–62. [CrossRef]
6. Wakashima, K.; Moriyama, T.; Mori, T. Steady-state creep of a particulate SiC/6061 Al composite. *Acta Mater.* **2000**, *48*, 891–901. [CrossRef]
7. Lin, Z.; Chan, S.L.; Mohamed, F.A. Effect of nano-scale particles on the creep behavior of 2014 Al. *Mater. Sci. Eng. A* **2005**, *394*, 103–111. [CrossRef]
8. Zhang, Q.; Zhang, W.; Liu, Y. Evaluation and mathematical modeling of asymmetric tensile and compressive creep in aluminum alloy ZL109. *Mater. Sci. Eng. A* **2015**, *628*, 340–349. [CrossRef]
9. Requena, G.; Degischer, H.P. Creep behaviour of unreinforced and short fibre reinforced AlSi12CuMgNi piston alloy. *Mater. Sci. Eng. A* **2006**, *420*, 265–275. [CrossRef]
10. Ma, Z.Y.; Tjong, S.C. Creep behavior of in-situ Al_2O_3 and TiB_2 particulates mixture-reinforced aluminum composites. *Mater. Sci. Eng. A* **1998**, *256*, 120–128. [CrossRef]
11. Ma, Z.Y.; Tjong, S.C. The high-temperature creep behaviour of 2124 aluminium alloys with and without particulate and SiC-whisker reinforcement. *Compos. Sci. Technol.* **1999**, *59*, 737–747. [CrossRef]
12. Li, Y.; Langdon, T.G. Creep behavior of an Al-6061 metal matrix composite reinforced with alumina particulates. *Acta Mater.* **1997**, *45*, 4797–4806. [CrossRef]
13. Matsuda, N.; Akaike, J.; Hongo, K.; Matsuura, K. The effect of second phase on the creep deformation of 6061Al matrix composites. *Mater. Sci. Eng. A* **1997**, *234*, 751–754. [CrossRef]
14. Requena, G.C.; Degischer, H.P. Effects of particle reinforcement on creep behaviour of AlSi1MgCu. *Z. Metallkd.* **2005**, *96*, 807–813. [CrossRef]
15. Spigarelli, S.; Evangelista, E.; Cucchieri, S. Analysis of the creep response of an Al-17Si-4Cu-0.55Mg alloy. *Mater. Sci. Eng. A* **2004**, *387–389*, 702–705. [CrossRef]
16. Shin, J.; Bae, D. Creep Properties in TiO_2 Nanoparticle Reinforced Aluminum Matrix Composites. *Adv. Eng. Mater.* **2013**, *15*, 1029–1033. [CrossRef]
17. Requena, G.C.; Degischer, P.; Marks, E.D.; Boller, E. Microtomographic study of the evolution of microstructure during creep of an AlSi12CuMgNi alloy reinforced with Al_2O_3 short fibres. *Mater. Sci. Eng. A* **2008**, *487*, 99–107. [CrossRef]
18. Deshmukh, S.P.; Mishra, R.S.; Kendig, K.L. Creep behavior of extruded Al-6Mg-1Sc-1Zr-10vol.% SiC_p composite. *Mater. Sci. Eng. A* **2005**, *410–411*, 53–57. [CrossRef]
19. Wang, L.; Qiu, F.; Zhao, Q.; Zha, M.; Jiang, Q. Superior high creep resistance of in situ nano-sized TiC_x/Al-Cu-Mg composite. *Sci. Rep.* **2017**, *7*, 4540. [CrossRef] [PubMed]
20. Dutta, B.; Surappa, M.K. Age-hardening behaviour of Al-Cu-SiC p composites synthesized by casting route. *Scr. Metall. Mater.* **1995**, *32*, 731–736. [CrossRef]
21. Siebeck, S.; Roder, K.; Wagner, G.; Nestler, D. Influence of Boron on the Creep Behavior and the Microstructure of Particle Reinforced Aluminum Matrix Composites. *Metals* **2018**, *8*, 110. [CrossRef]
22. Winand, H.M.A.; Whitehouse, A.F.; Withers, P.J. An investigation of the isothermal creep response of Al-based composites by neutron diffraction. *Mater. Sci. Eng. A* **2000**, *284*, 103–113. [CrossRef]
23. Krajewski, P.E.; Allison, J.E.; Jones, J.W. The effect of SiC particle reinforcement on the creep behavior of 2080 aluminum. *Metall. Mater. Trans. A* **1997**, *28*, 611–620. [CrossRef]
24. Fernández-Gutiérrez, R.; Requena, G.C. The effect of spheroidisation heat treatment on the creep resistance of a cast AlSi12CuMgNi piston alloy. *Mater. Sci. Eng. A* **2014**, *598*, 147–153. [CrossRef]
25. Fernández, R.; González-Doncel, G. Threshold stress and load partitioning during creep of metal matrix composites. *Acta Mater.* **2008**, *56*, 2549–2562. [CrossRef]

26. Jaglinski, T.; Lakes, R. Creep behavior of Al-Si die-cast alloys. *J. Eng. Mater.-Trans. ASME* **2004**, *126*, 378–383. [CrossRef]
27. Geng, J.; Hong, T.; Shen, Y.; Liu, G.; Xia, C.; Chen, D.; Wang, M.; Wang, H. Microstructural stability of in-situ TiB_2/Al composite during solution treatment. *Mater. Charact.* **2017**, *124*, 50–57. [CrossRef]
28. Shen, Y.; Li, X.; Hong, T.; Geng, J.; Wang, H. Effects of TiB_2 particles on microstructure and mechanical properties of an in-situ TiB_2/Al-Cu-Li matrix composite. *Mater. Sci. Eng. A* **2016**, *655*, 265–268. [CrossRef]
29. Ma, Y.; Chen, Z.; Wang, M.; Chen, D.; Ma, N.; Wang, H. High cycle fatigue behavior of the in-situ TiB_2/7050 composite. *Mater. Sci. Eng. A* **2015**, *640*, 350–356. [CrossRef]
30. Farkoosh, A.R.; Pekguleryuz, M. The effects of manganese on the T-phase and creep resistance in Al-Si-Cu-Mg-Ni alloys. *Mater. Sci. Eng. A* **2013**, *582*, 248–256. [CrossRef]
31. Han, G.; Zhang, W.; Zhang, G.; Feng, Z.; Wang, Y. High-temperature mechanical properties and fracture mechanisms of Al-Si piston alloy reinforced with in situ TiB_2 particles. *Mater. Sci. Eng. A* **2015**, *633*, 161–168. [CrossRef]
32. Ma, Z.Y.; Tjong, S.C. Creep deformation characteristics of discontinuously reinforced aluminium-matrix composites. *Compos. Sci. Technol.* **2001**, *61*, 771–786. [CrossRef]
33. Spigarelli, S.; Cabibbo, M.; Evangelista, E.; Langdon, T.G. Creep properties of an Al-2024 composite reinforced with SiC particulates. *Mater. Sci. Eng. A* **2002**, *328*, 39–47. [CrossRef]
34. Kloc, L.; Spigarelli, S.; Cerri, E. Behavior of an aluminum 2024 alloy produced by powder metallurgy. *Acta Mater.* **1997**, *45*, 529–540. [CrossRef]
35. Zhao, W.G.; Wang, J.G.; Zhao, H.L.; Yao, D.M.; Jiang, Q.C. High creep resistance behavior of the cast Al-Cu alloy modified by nano-scale PrxOy. *Mater. Sci. Eng. A* **2009**, *515*, 10–13. [CrossRef]
36. Zuo, L.; Ye, B.; Feng, J.; Kong, X.; Jiang, H.; Ding, W. Microstructure, tensile properties and creep behavior of Al-12Si-3.5Cu-2Ni-0.8Mg alloy produced by different casting technologies. *J. Mater. Sci. Technol.* **2018**, *34*, 1222–1228. [CrossRef]
37. Park, K.T.; Lavernia, E.J.; Mohamed, F.A. High temperature creep of silicon carbide particulate reinforced aluminum. *Acta Metall. Mater.* **1990**, *38*, 2149–2159. [CrossRef]
38. Cadek, J.; Oikawa, H.; Sustek, V.; Pahutova, M. High Temperature Creep Behaviour of Silicon Carbide Particulate Reinforced Aluminium. *High Temp. Mater. Process.* **1994**, *13*, 327–338. [CrossRef]
39. Park, K.T.; Mohamed, F.A. Creep strengthening in a discontinuous SiC-Al composite. *Metall. Mater. Trans. A* **1995**, *26*, 3119–3129. [CrossRef]
40. Krajewski, P.E.; Jones, J.W.; Allison, J.E. The effect of particle reinforcement on the creep behavior of single-phase aluminum. *Metall. Mater. Trans. A* **1995**, *26*, 3107. [CrossRef]
41. Li, Y.; Langdon, T.G. A comparison of the creep properties of an Al-6092 composite and the unreinforced matrix alloy. *Metall. Mater. Trans. A* **1998**, *29*, 2523–2531. [CrossRef]
42. Li, Y.; Mohamed, F.A. An investigation of creep behavior in an SiC-2124 Al composite. *Acta Mater.* **1997**, *45*, 4775–4785. [CrossRef]
43. Ryu, H.J.; Cha, S.I.; Hong, S.H. Generalized shear-lag model for load transfer in SiC/Al metal-matrix composites. *J. Mater. Res.* **2011**, *18*, 2851–2858. [CrossRef]
44. Pandey, A.B.; Mishra, R.S.; Mahajan, Y.R. Effect of isothermal heat treatment on the creep behaviour of an Al-TiC_p composite. *Mater. Sci. Eng. A* **1996**, *206*, 270–278. [CrossRef]
45. González-Doncel, G.; Fernández, R. Comments on "Creep behavior of in situ TiC_P/2618 aluminum matrix composite". *Mater. Sci. Eng. A* **2010**, *527*, 3288–3292. [CrossRef]
46. Kang, Y.C.; Chan, L.I. Tensile properties of nanometric Al_2O_3 particulate-reinforced aluminum matrix composites. *Mater. Chem. Phys.* **2004**, *85*, 438–443. [CrossRef]
47. Mazahery, A.; Shabani, M.O. Characterization of cast A356 alloy reinforced with nano SiC composites. *J. Nonferrous Met. Soc.* **2012**, *22*, 275–280. [CrossRef]
48. Erfanian-Naziftoosi, H.R.; Rincón, E.J.; López, H.F. Creep Properties of the As-Cast Al-A319 Alloy: T4 and T7 Heat Treatment Effects. *Metall. Mater. Trans. A* **2016**, *47*, 4258–4267. [CrossRef]
49. Dyson, B.F.; McLean, M. Particle-coarsening, σ_0 and tertiary creep. *Acta Metall.* **1983**, *31*, 17–27. [CrossRef]
50. Pandey, A.B.; Mishra, R.S.; Mahajan, Y.R. High-temperature creep of Al-TiB_2 particulate composites. *Mater. Sci. Eng. A* **1994**, *189*, 95–104. [CrossRef]
51. Karnesky, R.A.; Meng, L.; Dunand, D.C. Strengthening mechanisms in aluminum containing coherent Al3Sc precipitates and incoherent Al_2O_3 dispersoids. *Acta Mater.* **2007**, *55*, 1299–1308. [CrossRef]

52. Wang, S.; Luo, J.R.; Hou, L.G.; Zhang, J.S.; Zhuang, L.Z. Identification of the threshold stress and true activation energy for characterizing the deformation mechanisms during hot working. *Mater. Des.* **2017**, *113*, 27–36. [CrossRef]
53. Yong, L.I.; Langdon, T.G. Creep behavior of a reinforced Al-7005 alloy: Implications for the creep processes in metal matrix composites. *Acta Mater.* **1998**, *46*, 1143–1155.
54. Li, Y.; Langdon, T.G. Characteristics of creep deformation in discontinuously reinforced metal matrix composites. *Mater. Sci. Technol.* **2013**, *15*, 357–365. [CrossRef]